



Evaluation of full-scale laboratory models of geosynthetic reinforced pavement systems  
by Macgregor L Fogelsong

A thesis submitted in partial fulfillment of the requirements for the degree of Master of Science in Civil Engineering

Montana State University

© Copyright by Macgregor L Fogelsong (1998)

Abstract:

Geogrids and geotextiles have been used for more than 16 years as reinforcement in the base course layer of flexible pavements. Benefits from reinforcement include a possible reduction in the required thickness of the base course layer and an increase in the design life of the pavement.

Currently, mechanisms of reinforcement are not well understood and a quantitative evaluation of geosynthetic reinforcement effects on rutting behavior in flexible pavements is difficult.

21 full-scale laboratory models of flexible pavements systems were constructed and cyclically loaded. Both control (unreinforced) and reinforced sections were constructed and tested. Major variables included geosynthetic type, subgrade stiffness, base course thickness, and location of reinforcement.

Geogrid and geotextile reinforcement of the base layer over a soft clay subgrade showed improved rutting performance over comparable unreinforced sections. No significant performance differences were seen when a stiff silty-sand subgrade was used. Changes in major variables such as subgrade type, geosynthetic type, and base layer thickness resulted in significant performance differences. Geosynthetic reinforcement of the base layer appears to be a viable technology for improving rutting performance of flexible pavements over soft subgrades.

**EVALUATION OF FULL-SCALE LABORATORY MODELS OF  
GEOSYNTHETIC REINFORCED PAVEMENT SYSTEMS**

by

Macgregor L. Fogelsong

A thesis submitted in partial fulfillment  
of the requirements for the degree

of

Master of Science

in

Civil Engineering

MONTANA STATE UNIVERSITY-BOZEMAN  
Bozeman, Montana

December 1998

© COPYRIGHT

by

Macgregor Leroy Fogelson

1998

All Rights Reserved

N378  
F6869

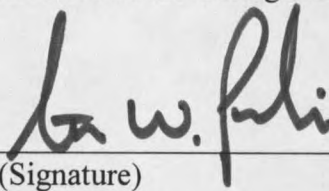
**APPROVAL**

of a thesis submitted by

Macgregor L. Fogelsong

This thesis has been read by each member of the thesis committee and has been found to be satisfactory regarding content, English usage, format, citations, bibliographic style, and consistency, and is ready for submission to the College of Graduate Studies.

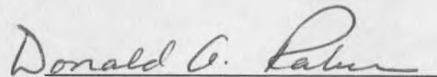
Dr. Steven W. Perkins

  
(Signature)

12-17-98  
(Date)

Approved for the Department of Civil Engineering

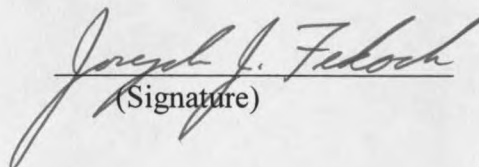
Dr. Donald Rabern

  
(Signature)

12/17/98  
(Date)

Approved for the College of Graduate Studies

Dr. Joe Fedock

  
(Signature)

12/17/98  
(Date)

## STATEMENT OF PERMISSION TO USE

In presenting this thesis in partial fulfillment of the requirements for a master's degree at Montana State University-Bozeman, I agree that the Library shall make it available to borrowers under the rules of the Library.

If I have indicated my intention to copyright this thesis by including a copyright notice page, copying is allowable for scholarly purposes, consistent with "fair use" as prescribed in the U.S. Copyright law. Requests for permission for extended quotation from or reproduction of this thesis in whole or in parts may be granted only by the copyright holder.

Signature



Date

12/17/98

## TABLE OF CONTENTS

	Page
<b>1. INTRODUCTION.....</b>	<b>1</b>
Background.....	1
Scope of Work.....	2
<b>2. REVIEW OF THE LITERATURE.....</b>	<b>4</b>
Introduction.....	4
Geosynthetic Functions.....	5
Filtration and Drainage Functions.....	6
Separation Function.....	6
Reinforcement Functions.....	8
Previous Experimental Work.....	12
Geogrid Reinforcement.....	12
Study Involving Geotextiles.....	23
Mixed Studies (Geogrids & Geotextiles).....	25
Conclusions.....	30
<b>3. EXPERIMENTAL METHODS.....</b>	<b>32</b>
Introduction.....	32
Laboratory Test Facility.....	33
Test Box and Loading Apparatus.....	33
Instrumentation.....	36
Asphalt Concrete Instrumentation.....	37
Geosynthetic Instrumentation.....	40
Base Course and Subgrade Instrumentation.....	41
General Instrumentation.....	43
Pavement Layer Materials.....	46
Asphalt Concrete.....	46
Base Course.....	46
Subgrade Materials.....	47
Geosynthetics.....	48
Test Section Construction.....	50

TABLE OF CONTENTS-Continued

	Page
Instrument Calibration.....	55
Instrument Installation.....	56
In-Situ Instrument Locations.....	61
Pavement Loading.....	63
As-Constructed Test Section Properties.....	64
Statistical Comparison of Test Section Properties.....	72
Instrument Measurement Repeatability.....	78
Construction and Loading of PCS1.....	79
Illustrations of Repeatability.....	80
<b>4. DISCUSSION OF RESULTS.....</b>	<b>89</b>
Introduction.....	89
Clay Section Behavior.....	90
Rutting Behavior.....	90
Lateral Base Restraint Mechanism.....	95
Improved Vertical Stress Distribution on Subgrade.....	101
Lateral Spreading on Top of Subgrade.....	103
Vertical Strain in Subgrade.....	104
Effect of Additional Base Material.....	105
Silty-Sand Subgrade Section Behavior.....	106
Rutting Behavior.....	106
Lateral Base Restraint Mechanism.....	107
Soil/Geosynthetic Compatibility.....	108
Subgrade Effects.....	109
<b>5. COMPARISON OF SINGLE-PULSE TEST RESULTS TO     LINEAR ELASTIC THEORY.....</b>	<b>147</b>
Introduction.....	147
KENLAYER Computer Program.....	148
Model Geometry and Determination of Pavement Layer Elastic Moduli.....	148
Comparison of Model Output to Section PCS1.....	152
Surface Deflections/AC Strain.....	153
Stress Predictions.....	155
Strain Predictions.....	156
Stress and Strain Beneath Load Centerline.....	157
Subgrade Strain Criterion Analysis.....	158

TABLE OF CONTENTS-Continued

	Page
Rut Development Predictions Using Empirical Relations.....	161
<b>6. CONCLUSIONS AND RECOMMENDATIONS.....</b>	<b>182</b>
Summary.....	182
Shear Resisting Interface Mechanism.....	184
Modeling Developments.....	188
Recommendations for Further Research.....	189
<b>BIBLIOGRAPHY.....</b>	<b>190</b>
<b>APPENDIX A.....</b>	<b>197</b>



## LIST OF TABLES

	Page
Table 2.1. Test section data from Haas et al. (1998) (from Perkins & Ismeik (1997a)).....	19
Table 2.2. Test section data from Brandon et al. (1995).....	28
Table 3.1. Geosynthetic material parameters.....	49
Table 3.2. Reinforcement placement for all test sections.....	51
Table 3.3. CBR results showing time variation for subgrades of sections SSS1-4. ....	65
Table 3.4. As-constructed subgrade properties.....	66
Table 3.5. As-constructed base course properties.....	67
Table 3.6. Coefficients of variation for base course and subgrade construction.....	70
Table 3.7. As-constructed asphalt concrete properties. ....	71
Table 3.8. One-way analysis of variance (ANOVA) for asphalt concrete voids in the SSS series tests.....	73
Table 3.9. One-way analysis of variance (ANOVA) for asphalt concrete voids in the CS series tests.....	74
Table 3.10. Post hoc comparison of mean voids for the SSS series of test sections .....	74
Table 3.11. Post hoc comparison of mean voids for the CS series of tests sections. ....	75
Table 3.12. Average load applied for all test sections completed .....	78

LIST OF TABLES-Continued

	Page
Table 4.1. Dynamic load induced in the geosynthetic.....	100
Table 5.1. Summary of model input parameters.....	152
Table 5.2. Empirical constants “x” and “y” and rut depth proposed by various agencies.....	160
Table 5.3. Comparison of empirical failure models (rutting) to CS2 and CS8. ....	160
Table 5.4. Comparison of experimental plastic strain parameters to parameters from Li et al. (1996). ....	165
Table A1. Sensor locations for test section SSS1.....	198
Table A2. Sensor locations for test section SSS2.....	200
Table A3. Sensor locations for test section SSS3.....	202
Table A4. Sensor locations for test section SSS4.....	204
Table A5. Sensor locations for test section SSS5.....	206
Table A6. Sensor locations for test section SSS6.....	208
Table A7. Sensor locations for test section SSS7.....	210
Table A8. Sensor locations for test section SSS8.....	212
Table A9. Sensor locations for test section SSS9.....	214
Table A10. Sensor locations for test section PCS1.....	216
Table A11. Sensor locations for test section CS1.....	218
Table A12. Sensor locations for test section CS2.....	220
Table A13. Sensor locations for test section CS3.....	222

LIST OF TABLES-Continued

	Page
Table A14. Sensor locations for test section CS5.....	223
Table A15. Sensor locations for test section CS6.....	225
Table A16. Sensor locations for test section CS7.....	227
Table A17. Sensor locations for test section CS8.....	229
Table A18. Sensor locations for test section CS9.....	231
Table A19. Sensor locations for test section CS10.....	233
Table A20. Sensor locations for test section CS11.....	235

## LIST OF FIGURES

	Page
Figure 2.1. Illustration of mixing of the base and subgrade, where addition of geosynthetic would be beneficial as a separator .....	7
Figure 2.2. Illustration of the tensioned membrane effect .....	9
Figure 2.3. Shear surface alteration resulting in an increased bearing capacity .....	10
Figure 2.4. Illustration of the lateral restraint concept.....	11
Figure 2.5. TBR versus base thickness for geogrid A and B (Collin et al. 1996).....	16
Figure 2.6. TBR versus rut depth based on results from Webster (1992) (from Perkins & Ismeik (1997a)). .....	17
Figure 2.7. TBR versus rut depth from results of Haas et al. (1988) (from Perkins & Ismeik (1997a)).....	20
Figure 2.8. TBR versus rut depth from results of Miura (1990) (from Perkins & Ismeik (1997a)).....	22
Figure 3.1. Isometric view of the test box and loading apparatus. ....	34
Figure 3.2. Schematic of apparatus components and pavement layers. Note: Load not shown in center of box to illustrate movement capabilities. ....	35
Figure 3.3. Overall picture of the pavement test facility .....	36
Figure 3.4. Closeup of the 305 mm diameter load plate, load cell (top), and surface LVDT's resting on the pavement surface.....	37

LIST OF FIGURES-Continued

	Page
Figure 3.5. Typical plot of permanent surface deformation after 5 load cycles for test section CS1 .....	38
Figure 3.6. Asphalt concrete strain gage.....	39
Figure 3.7. Different components of the Dynatest H-type PAST (Dynatest, 1991) .....	40
Figure 3.8. Large geotextile foil strain gage (top) and smaller geogrid foil strain gage (bottom).....	41
Figure 3.9. Dynatest SOil Pressure Transducer (SOPT) (Dynatest, 1991).....	42
Figure 3.10. Typical stress cell .....	43
Figure 3.11. Typical LVDT from RDP Electronics (Pottstown, PA).....	44
Figure 3.12. A view of the amplifiers used for all instruments and the corresponding onscreen output from Labview .....	45
Figure 3.13. Grain size distribution of cold-mix aggregate, hot-mix aggregate, base course, and silty-sand subgrade .....	47
Figure 3.14. Laboratory test CBR versus water content for the clay subgrade.....	49
Figure 3.15. Skid steer loader used for all soil mixing and lift placement .....	52
Figure 3.16. Vibratory plate compactor used for compaction of silty-sand subgrade, base course, and asphalt concrete .....	53
Figure 3.17. Troxler model 3411-B nuclear densometer.....	54
Figure 3.18. Dynamic cone penetrometer used for CBR determinations of pavement layer materials.....	54
Figure 3.19. Upright "jumping-jack" compactor used for compaction of clay subgrade.....	55

LIST OF FIGURES-Continued

	Page
Figure 3.20. Theoretical stress and strain measurements for an element of soil inside a test section.....	62
Figure 3.21. Input load pulse and corresponding load cell measurement.....	64
Figure 3.22. Dry density and water content versus depth from section SSS9 excavation.....	69
Figure 3.23. Peak vertical strain versus distance in the base layer for two soil strain sensors (LVDT's) from section PCS1 at two different positions ( $Z=300$ mm).....	81
Figure 3.24. Vertical strain versus radial distance from the load application from section PCS1 in the top of the subgrade ( $Z=450$ mm).....	82
Figure 3.25. Illustration of radial strain measures from two soil strain sensors in the top of the subgrade from section PCS1 ( $Z=415$ mm).....	83
Figure 3.26. Vertical stress distribution in the base layer from two stress cells from section PCS1 ( $Z=300$ mm).....	83
Figure 3.27. Vertical stress distribution in the subgrade from two stress cells from section PCS1 ( $Z=675$ mm).....	84
Figure 3.28. Permanent rut development for test sections CS2 and CS8.....	85
Figure 3.29. Long-term measures of radial strain in the base at a radial distance of 200 mm from the load centerline from test sections CS2 and CS8 ( $Z=325$ mm).....	85
Figure 3.30. Long-term dynamic vertical stress in the top of the subgrade from test sections CS2 and CS8 ( $R=0$ mm, $Z=450$ mm).....	86
Figure 3.31. Permanent radial strain in the base ( $R=150$ mm, $Z=215$ mm) (SSS1, SSS4).....	87

LIST OF FIGURES-Continued

	Page
Figure 3.32. Dynamic vertical stress versus cycle number in subgrade (R=0 mm, Z=350 mm) (SSS1, SSS4).....	87
Figure 3.33. Permanent vertical strain versus cycle number in subgrade (R=60 mm, Z=575 mm) (SSS1, SSS4).....	88
Figure 4.1. Permanent surface deformation versus cycle number for less than 80,000 cycles (CS2-CS11).....	111
Figure 4.2. Permanent surface deformation versus cycle number for all cycles (CS2-CS11).....	111
Figure 4.3. Permanent surface deformation versus cycle number (CS9, CS10).....	112
Figure 4.4. TBR for sections CS5, 6, 7, 9, and 11 relative to CS2.....	112
Figure 4.5. TRB for section CS10 relative to CS9.....	113
Figure 4.6. Permanent surface deformation bowls at cycle 1 (CS2-CS11).....	113
Figure 4.7. Permanent surface deformation bowls at cycle 40,000 (CS2- CS11).....	114
Figure 4.8. Permanent surface deformation bowls at cycle 1 (CS9-CS10).....	114
Figure 4.9. Permanent surface deformation bowls at cycle 125,000. (CS9- CS10).....	115
Figure 4.10. Surface dynamic deformation bowls at cycle 1 (CS2-CS11).....	115
Figure 4.11. Dynamic surface deformation bowls at a permanent rut depth of 12.5 mm (CS2-CS11).....	116
Figure 4.12. Dynamic surface deformation versus cycle number (CS2- CS11).....	116
Figure 4.13. Dynamic surface deformation versus cycle number (CS9, CS10).....	117

LIST OF FIGURES-Continued

	Page
Figure 4.14. Permanent radial strain in base of sections CS2-CS11. (R=100, Z=325mm) .....	117
Figure 4.15. Permanent radial strain in base of sections CS2-CS11. (R=200, Z=325mm) .....	118
Figure 4.16. Permanent radial strain in the base versus radial distance at cycle 1 of sections CS2-CS11 (Z=325mm).....	118
Figure 4.17. Permanent radial strain in the base versus radial distance at cycle 40,000 of sections CS2-CS11 (Z=325mm).....	119
Figure 4.18. Permanent radial strain versus cycle number in the base of sections CS9-CS10 (R=100mm, Z=400mm) .....	119
Figure 4.19. Permanent radial strain versus cycle number in the base of sections CS9-CS10 (R=200mm, Z=400mm) .....	120
Figure 4.20. Permanent radial strain versus radial distance in the base of sections CS9-CS10 at cycle 125,000 (Z=400mm).....	120
Figure 4.21. Dynamic radial strain in base of sections CS2-CS11 (R=100, Z=325mm).....	121
Figure 4.22. Permanent radial strain (M) in the geosynthetics of sections CS5-CS11 (R=15 mm).....	121
Figure 4.23. Permanent radial strain (XM) in the geosynthetics of sections CS5-CS11 (R=20 mm).....	122
Figure 4.24. Permanent radial strain in the geosynthetic (M) versus radial distance of sections CS5-CS11 at cycle 7,500. ....	122
Figure 4.25. Dynamic radial strain (M) in the geosynthetics of sections CS5-CS11 (R=15mm).....	123
Figure 4.26. Dynamic radial strain (XM) in the geosynthetics of sections CS5-CS11 (R=20mm).....	123



LIST OF FIGURES-Continued

	Page
Figure 4.27. Dynamic radial strain in the geosynthetic (M) versus radial distance of sections CS5-CS11 at cycle 1. ....	124
Figure 4.28. Dynamic radial strain in the geosynthetic (M) versus radial distance of sections CS5-CS11 at cycle 7,500. ....	124
Figure 4.29. Permanent vertical strain versus cycle number in the base beneath the load centerline (R=65mm) (CS2-CS11) .....	125
Figure 4.30. Dynamic vertical stress versus cycle number in the subgrade of sections CS2-CS11 (R=0, Z=450 mm) .....	125
Figure 4.31. Dynamic vertical stress versus cycle number in the subgrade of sections CS2-CS11 (R=0, Z=625 mm) .....	126
Figure 4.32. Dynamic vertical stress versus cycle number in the subgrade of sections CS2-CS11 (R=0, Z=775 mm) .....	126
Figure 4.33. Dynamic vertical stress versus cycle number in the subgrade of sections CS2-CS11 (R=0, Z=1075 mm) .....	127
Figure 4.34. Dynamic vertical stress versus cycle number in the subgrade of sections CS9-CS10 (R=200, Z=525 mm) .....	127
Figure 4.35. Dynamic vertical stress in the subgrade versus radial distance of sections CS2-CS11 at cycle 1. ....	128
Figure 4.36. Dynamic vertical stress in the subgrade versus radial distance of sections CS2-CS11 at cycle 40,000. ....	128
Figure 4.37. Permanent radial strain in the subgrade versus radial distance of sections CS2-CS11 at cycle 40,000. ....	129
Figure 4.38. Permanent radial strain versus radial distance in the subgrade of sections CS9-CS10 at cycle 125,000. (Z=490 mm).....	129
Figure 4.39. Permanent radial strain versus cycle number in the subgrade of sections CS9-CS10 (R=150mm, Z=490mm).....	130

LIST OF FIGURES-Continued

	Page
Figure 4.40. Permanent radial strain in the subgrade versus radial distance of sections CS2-CS11 at cycle 1. ....	130
Figure 4.41. Dynamic radial stress versus cycle number in the subgrade of sections CS9-CS10 (R=250, Z=525mm) .....	131
Figure 4.42. Permanent vertical strain versus cycle number in the subgrade of sections CS2-CS11 (R=65, Z=450 mm).....	131
Figure 4.43. Permanent vertical strain versus cycle number in the subgrade of sections CS2-CS11 (R=65, Z=625 mm).....	132
Figure 4.44. Permanent vertical strain versus cycle number in the subgrade of sections CS2-CS11 (R=65, Z=775 mm).....	132
Figure 4.45. Permanent vertical strain versus cycle number in the subgrade of sections CS2-CS11 (R=65, Z=1075 mm).....	133
Figure 4.46. Permanent vertical strain versus cycle number in the subgrade of sections CS9-CS10 (R=65, Z=525 mm).....	133
Figure 4.47. Permanent radial strain in the base versus radial distance of sections CS2, CS8, and CS9 at cycle 1. ....	134
Figure 4.48. Permanent radial strain in the base versus radial distance of sections CS2, CS8, and CS9 at cycle 40,000. ....	134
Figure 4.49. Dynamic vertical stress in the subgrade versus radial distance of sections CS2 and CS9 at cycle 1.....	135
Figure 4.50. Dynamic vertical stress in the subgrade versus radial distance of sections CS2 and CS9 at cycle 40,000.....	135
Figure 4.51. Permanent radial strain in the subgrade versus radial distance of sections CS2, CS8, and CS9 at cycle 1.....	136
Figure 4.52. Permanent radial strain in the subgrade versus radial distance of sections CS2, CS8, and CS9 at cycle 40,000 .....	136

LIST OF FIGURES-Continued

	Page
Figure 4.53. Permanent vertical strain versus cycle number in the subgrade of sections CS2, CS8, and CS9 (R=65) .....	137
Figure 4.54. Permanent surface deformation versus cycle number for sections SSS1-4 .....	137
Figure 4.55. Permanent radial strain vs. cycle in the bottom of asphalt layer at R=0 (SSS1-4) .....	138
Figure 4.56. Permanent radial strain in the base (R=150, Z=215 mm) (SSS1-4) .....	138
Figure 4.57. Permanent radial strain in the base (R=300, Z=215 mm) (SSS1-4) .....	139
Figure 4.58. Permanent radial strain in the base versus radial distance at cycle 500,000.(Z=160 mm) (SSS1-4) .....	139
Figure 4.59. Permanent vertical strain versus cycle number in the base beneath the load centerline. (R=60 mm) (Z=160 mm) (SSS1-4).....	140
Figure 4.60. Permanent radial strain (M) in the geosynthetics (R=15 mm) .....	140
Figure 4.61. Permanent radial strain (XM) in the geosynthetics (R=23 mm) .....	141
Figure 4.62. Distribution of peak radial strain in the geogrid and base course aggregate in section SSS5 at 5000 load cycles. ....	141
Figure 4.63. Distribution of permanent tangential strain in the geogrid and base course aggregate in section SSS5 at 5000 load cycles. ....	142
Figure 4.64. Distribution of permanent radial strain in the geotextile and base course aggregate in section SSS8 at 5000 load cycles. ....	142
Figure 4.65. Distribution of permanent tangential strain in the geotextile and base course aggregate in section SSS8 at 5000 load cycles. ....	143

LIST OF FIGURES-Continued

	Page
Figure 4.66. Distribution of peak radial strain in the geogrid and base course aggregate in section SSS2 at 5000 load cycles. ....	143
Figure 4.67. Dynamic vertical stress versus cycle number in the subgrade (R=0, Z=350 mm) (SSS1-4).....	144
Figure 4.68. Dynamic vertical stress versus radial distance in the subgrade at cycle 500,000. (Z=350 mm) (SSS1-4) .....	144
Figure 4.69. Permanent vertical strain versus cycle number in the subgrade (R=60 mm) (Z=350 mm).....	145
Figure 4.70. Permanent vertical strain versus cycle number in the subgrade (R=60 mm) (Z=575 mm) (SSS1-4) .....	145
Figure 4.71. Permanent vertical strain versus cycle number in the subgrade (R=60 mm) (Z=825 mm) (SSS1-4) .....	146
Figure 4.72. Permanent vertical strain versus cycle number in the subgrade. (R=60 mm) (Z=1075 mm) (SSS1-4) .....	146
Figure 5.1. Model geometry illustrating response levels corresponding to instrument depths.....	149
Figure 5.2. Peak elastic asphalt concrete surface deflection.....	167
Figure 5.3. Peak elastic radial strain versus radial distance in the AC (Z=67 mm).....	167
Figure 5.4. Peak elastic radial stress versus radial distance in the base (Z=225 mm).....	168
Figure 5.5. Peak elastic tangential stress versus radial distance in the base (Z=300 mm).....	168
Figure 5.6. Peak elastic radial stress versus radial distance in the base. (Z=300 mm).....	169

LIST OF FIGURES-Continued

	Page
Figure 5.7. Peak elastic vertical stress versus radial distance in the base (Z=300 mm).....	169
Figure 5.8. Peak elastic tangential stress versus distance in the subgrade (Z=450 mm).....	170
Figure 5.9. Peak elastic radial stress versus radial distance in the subgrade (Z=450 mm).....	170
Figure 5.10. Peak elastic vertical stress versus radial distance in the subgrade (Z=450 mm).....	171
Figure 5.11. Peak tangential stress versus distance in the subgrade (Z=675 mm) .....	171
Figure 5.12. Peak elastic radial stress versus radial distance in the subgrade (Z=675 mm).....	172
Figure 5.13. Peak elastic vertical stress versus radial distance in the subgrade (Z=675 mm).....	172
Figure 5.14. Peak elastic tangential stress versus distance in the subgrade (Z=675 mm) .....	173
Figure 5.15. Peak elastic radial strain versus radial distance in the base (Z=225 mm) .....	174
Figure 5.16. Peak elastic tangential strain versus radial distance in the base (Z=355 mm) .....	174
Figure 5.17. Peak elastic radial strain versus radial distance in the base (Z=355 mm) .....	175
Figure 5.18. Peak elastic vertical strain versus radial distance in the base (Z=300 mm) .....	175
Figure 5.19. Peak elastic tangential strain versus radial distance in the base (Z=355 mm) .....	176

LIST OF FIGURES-Continued

	Page
Figure 5.20. Peak elastic radial strain versus radial distance in the subgrade (Z=415mm).....	177
Figure 5.21. Peak elastic vertical strain versus radial distance in the subgrade (Z=450 mm).....	177
Figure 5.22. Peak elastic tangential strain versus distance in the subgrade (Z=415 mm) .....	178
Figure 5.23. Peak elastic radial strain versus radial distance in the subgrade (Z=675 mm).....	178
Figure 5.24. Peak elastic vertical strain versus radial distance in the subgrade (Z=675 mm).....	179
Figure 5.25. Peak elastic vertical stress versus depth at R=0 mm .....	179
Figure 5.26. Peak elastic radial stress versus depth at R=0 mm .....	180
Figure 5.27. Peak elastic radial strain versus depth at R=0 mm .....	180
Figure 5.28. Peak elastic vertical strain versus depth at R=0 mm .....	181
Figure 5.29. First cycle plastic strain parameter "A" as a function of the deviator stress/static stress ratio .....	181

## ABSTRACT

Geogrids and geotextiles have been used for more than 16 years as reinforcement in the base course layer of flexible pavements. Benefits from reinforcement include a possible reduction in the required thickness of the base course layer and an increase in the design life of the pavement.

Currently, mechanisms of reinforcement are not well understood and a quantitative evaluation of geosynthetic reinforcement effects on rutting behavior in flexible pavements is difficult.

21 full-scale laboratory models of flexible pavements systems were constructed and cyclically loaded. Both control (unreinforced) and reinforced sections were constructed and tested. Major variables included geosynthetic type, subgrade stiffness, base course thickness, and location of reinforcement.

Geogrid and geotextile reinforcement of the base layer over a soft clay subgrade showed improved rutting performance over comparable unreinforced sections. No significant performance differences were seen when a stiff silty-sand subgrade was used. Changes in major variables such as subgrade type, geosynthetic type, and base layer thickness resulted in significant performance differences. Geosynthetic reinforcement of the base layer appears to be a viable technology for improving rutting performance of flexible pavements over soft subgrades.

## CHAPTER ONE

### INTRODUCTION

#### Background

Geogrids and geotextiles have been used for more than 16 years as reinforcement in the base course layer of flexible pavements. Geotextiles were first used in unpaved haul roads in the late 1970's (Steward, et al. 1977), while geogrids were first studied in the late 1980's for reinforcement purposes (Haas et al. 1988; Barksdale et al. 1989). Use of these materials in the base course layer for reinforcement purposes is attractive from an economic point of view. Incorporating reinforcement into the base layer can benefit the roadway in two ways. The first benefit of reinforcement involves a possible reduction in the required thickness of the base layer. This alternative is attractive where thick base course layers may be needed over soft subgrades, or where gravel sources may be scarce. The second benefit exists when the reinforcement increases the design life of a pavement. This benefit is achieved through slower permanent rut development associated with geosynthetic reinforcement in the pavement system.

Specifically, the Montana Department of Transportation is interested in the use of the technology where low subgrade support values and thick base course layers are required, primarily in the eastern part of the state. In this area, quality aggregate sources



are scarce and haul costs of quality material are high. The intention of this research project is to provide data that for an interpretation of mechanisms by which geosynthetics increase pavement performance, and to provide a data base that will be used in developing a comprehensive Finite Element Model (FEM) of the reinforced pavement system. In the future, this model will be able to predict pavement response for different pavement layer properties as well as benefits from the inclusion of geogrids and geotextiles. Eventually, a design tool for geosynthetic reinforced pavements will be developed using test section data and FEM results.

### **Scope of Work**

The goal of this research was to evaluate the effects of geosynthetic reinforcement on the performance of laboratory-scale flexible pavement systems. This work was broken into five main tasks that coincide with five chapter divisions of this thesis. The tasks are listed and summarized below. It is noted that this thesis will neither include the finite element modeling work, nor the resulting design tool described above. These are future tasks in the overall research project that will be reported by others at a future date.

- Task 1: Conduct a thorough review of the literature to gain background information necessary for the successful implementation of a research program.

- Task 2: Design, build, and load laboratory-scale flexible pavement test sections incorporating informative variables such as geosynthetic type, subgrade strength, and base course thickness.
- Task 3: Synthesize results obtained from the experimental test sections and interpret the results pertaining to improvements in pavement performance.
- Task 4: Compare the stress/strain response of unreinforced test sections to layered linear elastic theory and to other published performance prediction models. This task should facilitate FEM development by exposing weaknesses in simpler modeling methods.
- Task 5: Conclude experimental results and comment on further research needed for the development of an accurate finite model and an effective design tool.

## CHAPTER TWO

### REVIEW OF THE LITERATURE

#### Introduction

The purpose of this chapter is to provide a review of concepts involved with geosynthetic reinforcement and to highlight experimental studies performed to date in this area of research. This chapter focuses mainly on laboratory-scale experiments using stationary cyclic loads or moving wheel loads in indoor test-track facilities, and on full-scale field studies involving vehicular traffic. The previous experimental work is critiqued with close attention given to important variables such as section layer thickness, pavement layer stiffness, geosynthetic type and stiffness, and geosynthetic placement within the section. Experimental results of numerous studies are summarized and critiqued. Benefits of reinforcement are at times described by the Traffic Benefit Ratio (TBR), defined as the ratio of the number of load cycles of a reinforced section to an identical unreinforced section necessary to achieve a particular rut depth. Unless noted, a 25 mm permanent surface deformation is used for TBR comparisons.

This chapter is divided into a review of geosynthetic functions and reinforcement mechanisms, and a review of previous experimental studies. At the conclusion of this chapter, an effort is made to combine the knowledge gained from previous experimental

results into a basis for the experimental program used in this research. The literature review will provide a basis for understanding previous problems encountered in this area of research and will illustrate important variables that will be incorporated into this thesis.

### **Geosynthetic Functions**

In order to quantify pavement behavior and response for unreinforced and geosynthetic reinforced situations, it is first necessary to understand the mechanisms thought to be responsible for reinforcement benefits and to understand other functions provided by geosynthetics. It is known that several mechanisms may contribute to improved performance, rather than a single mechanism. It is also known that different functions may occur between geotextile reinforced sections versus geogrid sections. The following sections will provide a deeper understanding of several main mechanisms believed to increase the performance of geosynthetic-reinforced roadways. These sections will also show why some reinforcement mechanisms do not account for reinforcement benefits in flexible pavement systems where rut depths are generally less than 25 mm.

Geotextiles and geogrids have several functions when used in roadways. Generally, four functions are used in describing the role of geosynthetics in roadways. These functions include separation, reinforcement, filtration, and drainage. Filtration and drainage will be described in general here, with specific descriptions of reinforcement and separation given hereafter.

### **Filtration and Drainage Functions**

Filtration and drainage functions can be considered to be similar. Filtration is defined as the ability of a geosynthetic to filter fines from the subgrade when water flows from the subgrade upward to the base. This water flow usually stems from excess pore water pressure development from either loading by traffic or freeze/thaw conditions. The purpose of the geosynthetic in this function is to filter the fines that would migrate into the base layer due to the flow of water. This condition could reduce the thickness of the subgrade and/or reduce the strength of the base layer, leading to a higher rut development rate than would otherwise be present without the geosynthetic.

The drainage function refers to a geosynthetic's ability to drain water from the pavement layer materials to the edge of the pavement. Drainage water can originate from the base layer (water intrusion laterally or from the AC surface) or from the subgrade layer, provided that excess pore water pressures are developed. Excess water in a pavement can lead to a reduction in effective stresses in the subgrade, causing increased rutting of that layer. The function of the geosynthetic then, is to provide a mechanism to route the water to the edge of the pavement, reducing the chance of rutting.

### **Separation Function**

The main difference between a soil separation function and a reinforcement function is that the latter provides a mechanical improvement of the soil. The separation function defines a geosynthetic's ability to maintain physical separation between the base and subgrade layers of a flexible pavement system. Separation prevents mixing of the

base and subgrade materials. Mixing is usually caused by construction techniques, which may push aggregate from the base into the subgrade. Another cause of mixing is from post-construction, cyclic loading due to traffic. Cyclic loading from traffic causes the subgrade fines to be squeezed into the aggregate of the base layer. Once the base is contaminated with these fines, frictional characteristics between aggregate particles are reduced. The reduction in frictional characteristics of the base reduces the strength and stiffness of the layer and promotes rutting. Rutting is promoted from a loss of support by the base leading to a more critical state of stress on the usually weaker subgrade layer. Potential benefits of geotextiles combine the separation and reinforcement functions. The separator can reduce intermixing while the reinforcement increases load carrying capacity. Figure 2.1 illustrates the situation where a geosynthetic would be beneficial as a separator in preventing mixing of the base and subgrade layers.

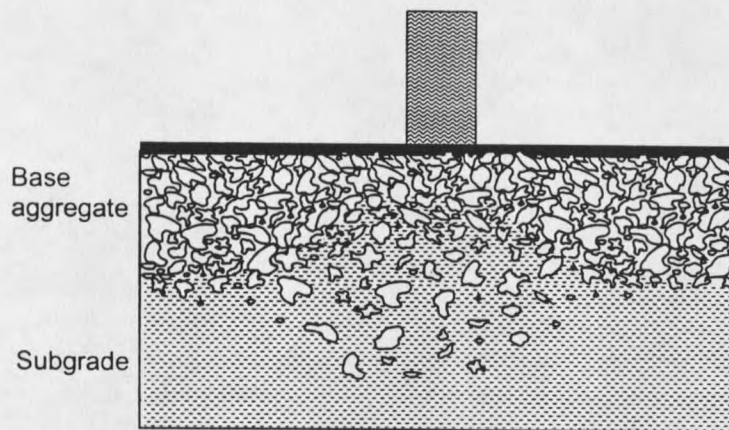


Figure 2.1. Illustration of mixing of the base and subgrade, where addition of geosynthetic would be beneficial as a separator.

## Reinforcement Functions

Two main reinforcement mechanisms are thought to be accountable for increasing the capacity of a geosynthetic reinforced roadway: the tensioned membrane mechanism, and the lateral restraint mechanism. Most reinforcement functions fall under these two categories. Many times, reinforcement effects are combined with one of the functions described previously. For example, reinforcement could be combined with a drainage or filtration function. It is often difficult to distinguish analytically or quantitatively between the rutting behavior of a pavement and the function(s) responsible for the behavior.

The tensioned membrane reinforcement mechanism requires locally applied loading and significant deformation of the pavement layers. Significant deformation is required to develop enough tension in the geosynthetic material to provide a net uplifting force. This level of deformation (usually much greater than 25 mm of rut), is not tolerable in flexible pavement systems, in contrast to unpaved or haul roads where this function may be more significant, as the large rut depths required by the mechanism are tolerable. In general, a stress reduction is achieved on the underlying soil beneath the applied load due to the uplift force provided by the tensioned membrane effect (Figure 2.2). Stress reduction provided by the geosynthetic leads to a less critical state of stress, which reduces the amount of rutting on the subgrade.

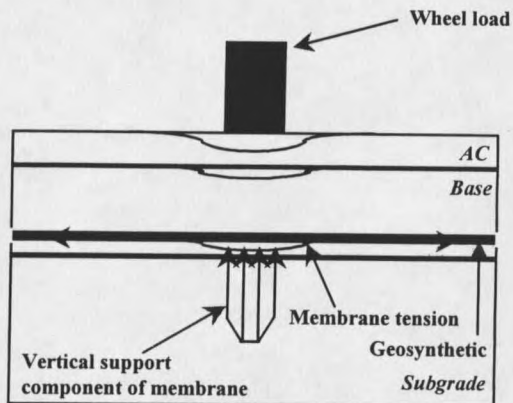


Figure 2.2. Illustration of the tensioned membrane effect.

Sometimes included in the tensioned membrane reinforcement concept is an increased bearing capacity function. The increased bearing capacity function essentially resists lateral displacement of the foundation soil (subgrade in this case) by restraining the lateral thrust in the fill (base layer). This function essentially alters the failure shear surface and forces a less critical failure surface to develop, usually above the level of the geosynthetic. This shear failure alteration is shown in Figure 2.3. Unfortunately for flexible pavement systems, the increased bearing capacity concept implies that the shear surface alteration is provided when the system is on the verge of failure or significant rut has developed, which as mentioned previously, cannot be tolerated by a flexible pavement system.



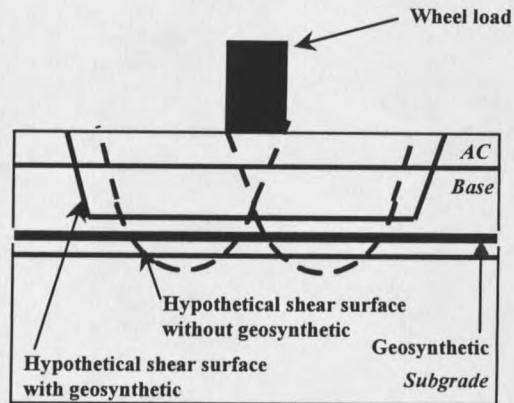


Figure 2.3. Shear surface alteration resulting in an increased bearing capacity.

The second and most probable reinforcement mechanism believed to account for increased performance of geosynthetic reinforced flexible pavements is that of lateral restraint. Lateral restraint is induced by frictional interaction (through direct friction or interlock in the case of geogrids) of the geosynthetic and surrounding soil. For this mechanism to be present, adequate friction must develop between the geosynthetic and the soil. In the case of geogrids, interlock of particles through the aperture of the grid provides adequate frictional resistance. For geotextiles, either direct frictional resistance between the soil and the material must be sufficient, or the reinforcement material must deform slightly into the subgrade soil to provide a dimpled effect (only in the case of low strength soils), resulting in satisfactory frictional characteristics.

Vertical, cyclic loading induces lateral spreading of the base course, which in turn induces tension in the geosynthetic. Load is transmitted from the surrounding soil into the geosynthetic. As the tension increases in the geosynthetic, the material confines the base material and increases the mean stress in the layer. With an increase in mean stress,

the base becomes “stiffer” and limits the shear failure mode. Another benefit of the base becoming “stiffer”, is that load spreading characteristics of the base layer are improved. As load is spread more evenly across the subgrade, a less critical state of stress is developed, reducing rutting.

Additionally, the lateral restraint provided by the geosynthetic reduces the lateral spreading of the base aggregate, thereby reducing the subsequent vertical deformation, which would have normally occurred without the geosynthetic reinforcement being present. The mechanism also reduces the shear stress on the top of the subgrade, and spreads the load over the subgrade. The reduction in shear stress and lateral spreading reduces the net vertical strain experienced by the subgrade. The lateral restraint mechanism is believed to occur with small vertical deformations in the pavement system, which makes it ideal for flexible pavement applications. Figure 2.4 illustrates the lateral restraint concept.

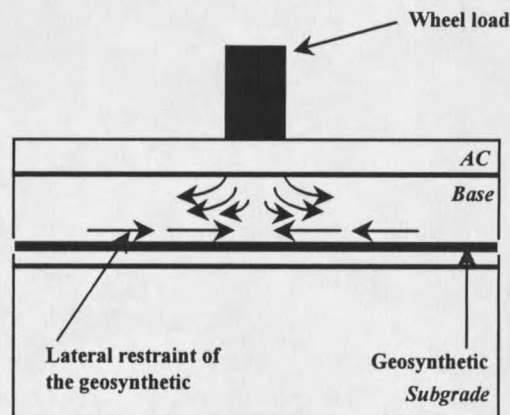


Figure 2.4. Illustration of the lateral restraint concept.

### Previous Experimental Work

This section provides an examination of previous experimental work. This research includes experiments performed at the laboratory scale involving stationary, cyclic loads and field-scale experiments involving vehicular traffic. Also provided is a description of test sections including critical design parameters such as section thickness, geosynthetic location, geosynthetic type, subgrade strength, and loading conditions. Previous experimental work is critiqued if it is believed that the methods affected the outcome of the study significantly. Results, whether showing improvement or not, are also contrasted with other findings to provide a basis for the research performed as part of this study. The previous experimental work will be divided into three categories: 1) studies involving geogrid reinforcement, 2) studies involving geotextile reinforcement, and 3) mixed studies involving both geogrids and geotextiles.

#### **Geogrid Reinforcement**

The effect of geogrid reinforcement in model track tests was studied by Moghaddas-Nejad & Small (1996). The loading carriage provided a 210 kPa (30 psi) load over a 24.5 cm<sup>2</sup> contact area. The wearing course consisted of a cold-mix (proprietary Pavifix) which had a maximum aggregate size of 5 mm. This material was chosen as to be a prototype of ¼ scale of real asphalt concrete aggregate. Base course material was an A-1-a or SP uniform fine gravel. D<sub>10</sub> and D<sub>60</sub> were 2.0 and 4.0 mm respectively. A-3 silica sand was used for the subgrade material. A Tensar SS2 geogrid was used for reinforcement (apertures of 40 mm and 28 mm in the longitudinal and

transverse directions). Thicknesses of the asphalt concrete, base, and subgrade were 20 mm, 40 mm, and 2000 mm respectively. Measurements were taken at the top of the asphalt layer (surface deformation), the top of the base course, and the top of the subgrade in only the vertical direction with LVDT's. The geogrid was not instrumented.

The authors showed that a geogrid placed in the middle of the base provided the best performance (70% reduction in surface deformation) for single-track and multiple-track tests with respect to surface deformation. This configuration also provided the smallest base course vertical displacement. Single-track loading was defined as a single unique path along which the wheel load traveled. The multiple-track tests included a sequence of nine random paths along which the wheel could travel, spaced 25 mm apart. The authors tried to disprove the tensioned membrane mechanism and showed that the maximum vertical geogrid deformation was less than 2mm, which they believed was insufficient to mobilize the membrane effect. They also showed that improvement of reinforced sections was substantial even at the point of only 100 load applications, where surface deformation was approximately 2-3 mm. Improvement over a small number of load cycles implies that the reinforcement was engaged immediately, rather than after large deformations as the tensioned membrane theory requires. The authors stated lateral confinement and interlocking with the base layer reduced the vertical displacement of the base layer, and acted as a "slab" in spreading the load to the subgrade. As the geogrid aperture size and stiffness was much larger than the aggregate size in the base layer of the proposed scaled down model, results in this study (with respect to improvement TBR ratios) may have been magnified somewhat due to scale effects.

A full-scale laboratory test on geosynthetic reinforcement of paved roads was conducted by Cancelli et al. (1996). A 1.8 m x 0.9 m x 0.9 m box was filled with 450 mm of Ticino siliceous sand, 300 mm of crushed limestone base with a maximum particle size of 30 mm, and 75 mm of asphalt concrete. The box was divided into two halves to construct and load both a control and a reinforced section at the same time. A 5 or 10 Hz load of 570 kPa was applied to the pavement surface through a 300 mm diameter plate, similar to that described in Haas (1986). Tests were constructed at subgrade California Bearing Ratio's (CBR) ranging from 1-18. Pavement sections were loaded to rather high deformations, up to 150 mm (2 inch). Several different types of geosynthetics were used in this research, which included multilayer biaxially oriented polypropylene geogrids, punched, biaxially-oriented polypropylene geogrids, biaxially oriented polypropylene geogrids manufactured by extrusion and orientation processing, polyester woven geogrid, and a slit film woven polypropylene geotextile.

Cancelli, et al. (1996) found that a punching shear failure near the edge of the load plate occurred in the AC layer in most tests. Reinforced sections exhibited less of the shear failure phenomena due primarily to better load spreading by the geogrid shown by permanent rut geometry across the pavement surface. Approximate traffic benefit ratios (at 25 mm rut depth) ranged from 1.53 (Amoco 6070) to 6.2 (Tenax LBO301) for a subgrade CBR of 3.0. Traffic benefit ratios (25 mm rut) ranged from 10-100 for several geogrids for a subgrade CBR=1.0. In addition, they found that improvement defined by TBR's increased for increasing rut depths, usually over 25 mm. The authors also showed that a geogrid reinforced section with a 300 mm base course performed slightly better in

terms of permanent deformation than an unreinforced section with a 400 mm base course. Results such as this provide promise for the use of the reinforcement technology where gravel is costly or scarce.

Another large loading facility was designed at the University of Alaska (Collin et al., 1996). The test facility consisted of a box 1.2 m deep, 2.4 m wide and 14.6 m long. A 20 kN load was applied by a rolling tire in one direction, and 9 kN in the opposite direction ( $180^{\circ}$ ). Four tests involving stiff geogrids (Tensar BX-1100, 'Geogrid A' and Tensar BX-1200, 'Geogrid B') were constructed. Two tests involved placing the geogrid at the subgrade/base course interface and a third involved two geogrids placed at the interface and within the base course. The final section was an unreinforced control section. Asphalt thickness was 50 mm, base course thickness was 150-460 mm, and the subgrade was 200-500 mm in thickness. Average subgrade CBR was 1.9.

The authors found that the stiffer BX-1200 (5% secant modulus=320 kN/m MD) performed better than a less stiff BX-1100 (5% secant modulus=211 kN/m). They found the stiffer geogrid to be more sensitive to base thickness. TBR ratios obtained from this research ranged from 1.8-10 for 175-300 mm base courses constructed on subgrade CBR's of 3.0. A maximum TBR of 10.0 was obtained from the BX-1200 geogrid with a 250 mm base, as shown in Figure 2.5. The authors obtained TBR's similar to those of Haas (1985) (TBR=2.7-3.0 for geogrid A) and Webster (1992) (TBR=4.7 for geogrid B).

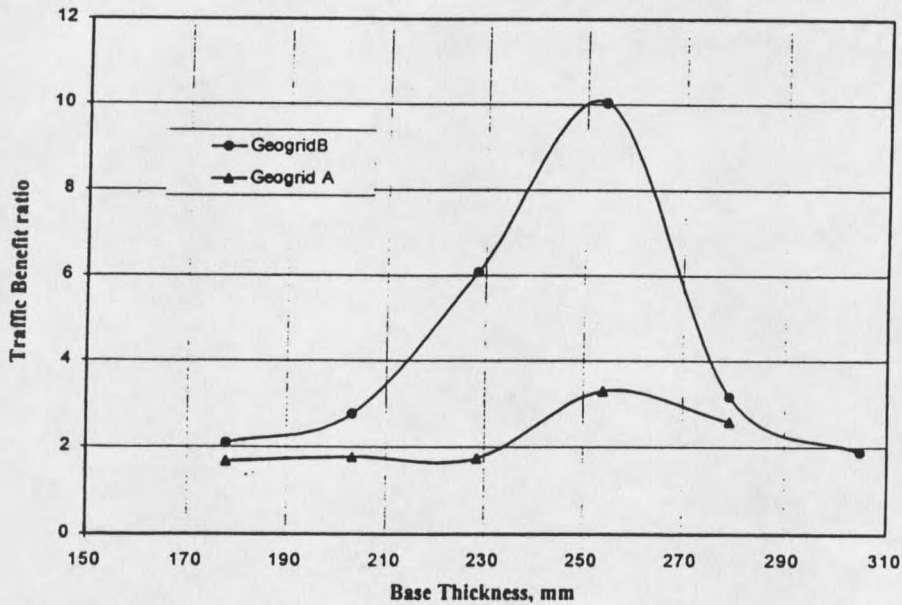


Figure 2.5 TBR versus base thickness for geogrid A and B (Collin et al. 1996).

Webster (1992) investigated the use of geogrids in reinforcing base courses for flexible pavements for light aircraft in full-scale field test sections. Webster investigated the importance of geogrid stiffness using a Tensar BX-1100 and BX-1200 geogrid. The subgrade consisted of a heavy clay (CH) material. CBR strengths of 3 and 8 were tested to be representative of low and high strength subgrades. A crushed limestone base course was used containing 12.3 % fines, which was considered to be low quality. All tests utilized a 50 mm AC surface, with maximum aggregate size of 12.7 mm and minimum Marshall Stability of 1500 lbs. It was noted that asphalt thickness varied from 56 mm to 66 mm thick, and averaged 61 mm thick. The geogrids specimens were not instrumented.

Webster did not observe any mixing between the base and subgrade. A TBR of 23 (at a permanent deformation of 25 mm) was obtained with the Tensar BX-1200 geogrid, corresponding to a base thickness of 152 mm and a CBR of 8. Initial elastic pavement deformations of reinforced versus unreinforced sections showed virtually no differences, implying that long-term effects such as the geogrid strength and creep properties may have influenced long-term deformation behavior.

Of interesting note from this study is that the maximum TBR values (based on 25 mm rut depth) were obtained with thin bases (150 mm to 200 mm). Figure 2.6 below summarizes several sections of varying base thickness with respect to TBR. In all cases, the geogrid was placed at the subgrade-base interface. Webster also found that the stiffer Tensar BX-1200 geogrid provided the best performance.

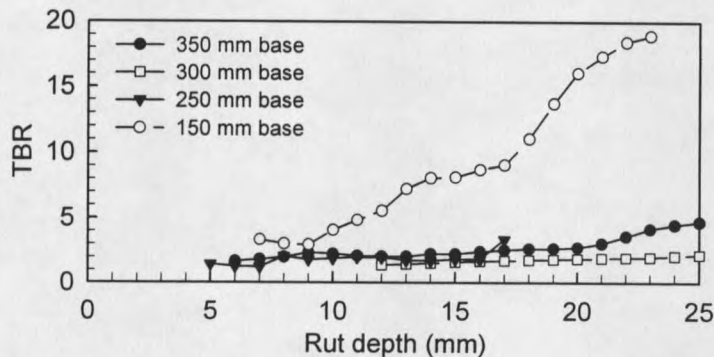


Figure 2.6. TBR versus rut depth based on results from Webster (1992) (from Perkins & Ismeik (1997a)).



Haas et al. (1988) utilized a 4.6 m x 1.8 m x 0.9 m box for an experimental test section. Loading was applied through a 300 mm diameter steel plate at a pressure of 550 kPa (80 psi). Loading frequency was 8 Hz. Dial gages were placed on the asphalt surface to measure surface deflections. Geogrids were instrumented with foil strain gages. Pressure cells were placed at the top of the subgrade in selected test sections.

Test variables included depth of reinforcement placement within the base course, base course thickness, and subgrade strength. Subgrade CBR strengths ranged from <1 to 8.0. A beach sand subgrade was used for all experiments, with some sections containing peat to yield low CBR values. Various CBR values were obtained by varying the water content. A Tensar BX-1100 geogrid was used for all tests.

Haas et al. (1988) concluded that geogrids may provide a TBR of up to 3.0 when properly located within the base course. The authors suggested that the optimal geogrid placement is at the bottom of thinner base courses and tending toward mid-base for thicker sections. Analysis of vertical stress induced on the top of the subgrade, strain in the geogrid, and surface deflection data showed that the load distribution characteristics of reinforced sections were quite different from unreinforced sections. Haas et al. (1988) also recommended placing the geogrid in a zone of moderate tensile strain (0.05-0.2% dynamic strain) and that permanent strain should not exceed 1-2%. It is the opinion of the author of this paper that this recommendation was made in order to prevent extensive plastic deformations of the geogrid from contributing to excess lateral deformation of the base layer. Excessive lateral deformations would lead to larger vertical deformations,

which are not desirable. In this case, a stiffer geogrid should be used which resists permanent strains better.

Table 2.1 gives section data for selected test sections from Haas et al. (1988). Figure 2.7 illustrates the TBR (for increasing rut depths) versus rut depth for the sections listed in Table 2.1. It is noted that the best results were obtained with the weakest subgrade conditions and placement of the geogrid at the mid-base position. Results with the same subgrade conditions but thinner base and placement of the geogrid at the base/subgrade interface provided the lowest TBR values. The differences between these two sets of sections implies that section thickness design and placement of the geogrid in a strain region as to not over strain the geogrid is very important. TBR values obtained from the stronger subgrade (sections 1 and 3) were high, which indicates there may be some validity to the use of geogrid reinforcement in cases of stiffer subgrades. Differences between TBR values between sections 11,12 and 15,16 may not be significant enough to determine effects of geogrid placement and/or reinforcement effects between subgrade strength differences.

Table 2.1 Test Section data from Haas et al. (1988) (from Perkins & Ismeik (1997a)).

Section	Geosynthetic Position	AC thickness (mm)	Base thickness (mm)	Subgrade CBR
1	Unreinforced	100	200	8
3	Middle of base	100	200	8
5	Unreinforced	75	300	1
6	Middle of base	75	300	1
11	Unreinforced	75	200	3.5
12	Bottom of base	75	200	3.5
15	Unreinforced	75	200	1
16	Bottom of base	75	200	1

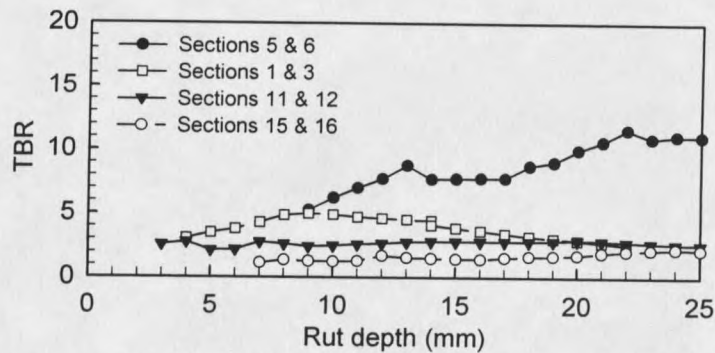


Figure 2.7. TBR versus rut depth from results of Haas et al. (1988) (from Perkins & Ismeik (1997a)).

As a summary, Haas (1988), suggested that a geosynthetic should provide appropriate interlock and should possess the following mechanical properties:

- 1) High tensile modulus to resist stretching under the load;
- 2) Dimensional stability to resist radial stresses without deforming, warping, or stretching;
- 3) Elastic response under dynamic loading (i.e small permanent strain development);
- 4) Resistance to plastic strain with repeated load applications;
- 5) Inertness and durability

Miura et al. (1990) conducted studies at both model and full-scale investigating the effects of geogrid reinforcement on soft clay subgrades (CBR=4-6). Materials investigated were Tensar BX-1200, and BX-1300 geogrids. Model tests were constructed in a box measuring 150 cm x 150 cm x 100 cm in depth. Model tests incorporated section thicknesses of 5 cm of asphalt, 35 cm of base, and 60 cm subgrade. Asphalt surface deformation was monitored via dial gages, and vertical pressure cells

were installed in the subgrade. Geogrid reinforcement was instrumented with strain gages. The model tests showed the BX-1200 geogrid to be most effective in reducing vertical surface deformation. Optimal placement for the grid was at the top of the subgrade, between the subgrade and base layers. The TBR's obtained at a deformation of 5 mm was 2.0-2.4 for the BX-1200 placed at the top of the subgrade and the subbase respectively. Interlocking and the tensioned membrane effect were noted for mechanisms responsible for behavior, but the authors believed placement in the field would not be appropriate to engage the tensioned membrane effect. Overall, not much difference was seen with placement depth.

Field tests by Miura (1990), incorporated section thicknesses of 5 cm, 15 cm, 20 cm (asphalt, base, and subbase) and a very large thickness of subgrade. The base course thickness was reduced by 5 cm for reinforced sections. From long-term results (6 months), it was concluded that the addition of a one-layer geogrid (BX-1200) was equivalent to 10 cm of base course. Figure 2.8 below shows section 4 (CBR=6, reinforced with Tensar BX-1300 geogrid, 20 cm base) and section 6 (CBR=4, reinforced with Tensar BX-1200 geogrid, 20 cm base) described by TBR versus depth. Fairly high TBR values were obtained with the two reinforced sections (TBR 5-17) with the sections performing relatively equal at higher rut depths. It is noted that the TBR decreases with increasing rut depth, which is contrary to the findings of both Haas et al. (1988), and Webster (1992). Both of those studies indicated increasing TBR with increasing rut depth. Apparently, some of the operating mechanisms or load distribution characteristics of the test sections are different between Miura (1990) and the other studies. The only

difference noticed was that Miura (1990) used a sub-base making the test sections a four-layer system. The four-layer system may have changed the load distribution characteristics of the section to cause the opposite trend of decreasing TBR with increasing rut depth.

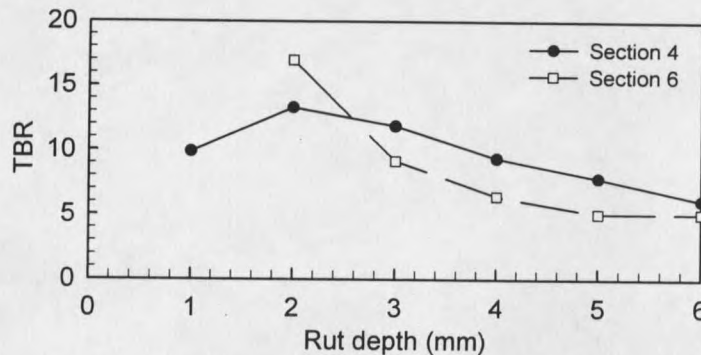


Figure 2.8. TBR versus rut depth from results of Miura (1990) (from Perkins & Ismeik (1997a)).

Kinney et al. (1998) and Kinney & Schuler (1998) developed an experimental program similar to earlier programs (Collin et al. 1996) using a moving cart providing a 550 kPa (80 psi) tire pressure to 61 mm of asphalt concrete. Subgrade soil was an alluvial sand and gravel mixed with additional silt and water to provide a CBR of on the order of 1.0. Variables in the study were base course thickness, tire pressure, and geogrid type. The two geogrids utilized (Tensar BX-1100 and BX-1200) had modulus values of 197 kN/m and 270 kN/m respectively. The BX-1100 geogrid had 39% open area (apertures) while the BX-1200 had 70% open area.

Experimental results showed geogrid reinforcement improved rut behavior for base course thicknesses up to 400 mm thick. For thicker bases, reinforcement provided

no additional improvement. As expected, lower tire pressure (225 kPa versus 550 kPa) provided slightly higher TBR values and less rutting when compared to the control. For a tire pressure of 550 kPa (80 psi), the BX-1100 provided a TBR from 6-10 for a 200 mm thick base, a TBR of 4.5 for a 280 mm base, and a TBR of approximately 2.0 with a 360 mm thick base. Response was fairly linear between those three points. For the same conditions, the BX-1200 geogrid had a much steeper TBR versus base course depth curve, indicating that the stiffer material had a better benefit for the same base course thickness. For a 250 mm thick base course, the BX-1200 provided a TBR of 10, a TBR of 7.5 for a 280 mm base, and a TBR of 2 for a 360 mm base. The TBR versus depth of base was nonlinear for the stiffer BX-1200 geogrid. Additionally, deflection basins (rut depth versus distance from the applied load) showed mixed results between the control, BX-1100 geogrid, and BX-1200 geogrid for a thick 360 mm base course. Deflection profiles for thinner (235 mm base) showed the stiffer BX-1200 to have a smaller peak deflection and less-steep sides to the basin, than the BX-1100 and the control. These experimental results seem to indicate a stiffer geogrid may provide a longer pavement life or significant savings of gravel when used in thinner bases. It remains to be seen whether economic implications will negate the better performance of the stiffer geogrid.

### **Study Involving Geotextiles**

A study by Halliday & Potter (1984), concluded that the incorporation of a woven polyester geotextile (ultimate strength 83 kN/m) at the base course/subgrade interface of

both a macadam (bitumen reinforced) surfaced and granite base course (unsurfaced) did little to improve the permanent deformation of the pavement. The authors constructed laboratory-scale sections on a low-strength subgrade (CBR=2.5). Loading was provided by rolling lorries on a test track and sections were loaded to approximately 75,000 standard axle loads. Measurements were taken of subgrade vertical stress, vertical strain, and transverse strain. Longitudinal and transverse strains were measured in the base course. Macadam surface thicknesses evaluated were 160 mm and 220 mm. Granite base course thickness was 300 mm. Asphalt surface thickness was variable due to variations in optical level measurements.

It was noted in all experimental measurements that results were clearly correlated to the thickness of the asphalt concrete layer, which had a variation in thickness throughout the sections. It was also noted that longitudinal and transverse strains at the bottom of the layer were unaffected by the inclusion of a geotextile which may provide insight into a geotextile providing poor lateral confinement due to shear interaction with the base course particles. Transient vertical stress and strain in the subgrade soil was also unaffected by the geotextile. The authors did note, however, that construction was easier with the geotextile, which provided a separation function between reinforced and unreinforced sections. 70 mm of contamination from the subgrade into the base course was seen in the control sections, which may be a function of construction techniques and/or loading conditions. This mixing was attributed to compaction. Additional material was needed in the control sections to provide the same total thickness due to the 70 mm of mixing.

### **Mixed Studies (Geogrids and Geotextiles)**

Large-scale laboratory experiments, involving both geotextiles and geogrids were carried out by Barksdale (1989). A 4.9 m x 2.4 m linear test track utilized a 7 kN wheel load moving at 4.8 kilometers per hour. Up to 70,000 loads were applied to the pavement surface. Contact pressures were between 462 kPa (67 psi) and 504 kPa (73 psi).

With very weak sections (CBR < 3.0), inclusion of a stiff geotextile at the bottom of the base course reduced the amount of surface rut by 44% compared to a control section. Barksdale also found that a major portion of the total deformation occurred within the aggregate base. Permanent deformation in the subgrade was small compared to that in the base course. The author illustrated a trend of large permanent vertical strain at the top of the base course decreasing rapidly with depth towards the subgrade. Barksdale found a decrease of permanent strain in the top of the subgrade but an increase in vertical strain in the top of the base course, when comparing the reinforced section to control sections. Another interesting point related to reinforcement effects on the subgrade, showed that only the top 150-180 mm of the subgrade were affected (i.e. differences in stress and strain in the material).

With respect to geosynthetic placement within the base, a geotextile (750 kN/m, at 5% strain) placed at the subgrade/base interface had a 57% reduction in the permanent deformation in the subgrade but only a 3% reduction in the base. A geotextile placed in the middle of the base reduced permanent base deformation by 31% and permanent subgrade deformation by only 14%. A geogrid placed at the interface did not decrease permanent deformation in the base (measurements showed a 5% increase), and showed a



52% improvement in permanent subgrade deformation. He found a geogrid of less stiffness (300 kN/m at 5% strain) compared to a geotextile (stiffness=750 kN/m at 5% strain) placed at mid-base performed better (6.6 mm rut with the textile compared to 4.6 mm rut with the geogrid) than the geotextile.

For a typical pavement section designed for 2,000,000 ESALs (AC thickness 165 mm, base thickness =165 mm, subgrade modulus=24,000 kPa), Barksdale et al. (1989) showed from analytical model predictions little or no improvement in stress/strain distributions and rutting with the inclusion of a geosynthetic.

In summary, Barksdale et al. (1989) recommended minimum stiffnesses for a geogrid of 260 kN/m and 700 kN/m for a geotextile (5% strain secant moduli) to be used with subgrades of  $CBR < 3.0$ , and recommended placement of the reinforcement at the base/subgrade interface. Barksdale et al. (1989) also stated that little improvement was seen for an AC thickness greater than 65 mm based on his evaluation of the design 2,000,000 ESAL experimental tests. The stated reason for geosynthetic improvement of pavements was that the presence of a geosynthetic caused a small increase in confining stress and reduction in vertical stress in the base and in the upper 150-180 mm of the subgrade. This statement may imply that the lateral restraint mechanism was involved in improvement. The lateral restraint may have increased the stiffness of the base and may also be the reason for a decrease in vertical stress on the subgrade. Without further quantitative analysis, the determination of the lateral restraint mechanism being solely responsible for improvement is difficult at best.

Al-Qadi et al. (1994) conducted laboratory studies of geosynthetic reinforced pavements in a test box measuring 3.1 x 1.8 x 2.1 m deep. Subgrade material was a Yatesville silty-sand with a CBR strength of 4.0. 70 mm of AC surfacing was placed over 150 mm of basecourse. Amoco 2002 and 2016 geotextiles (5% strain 8.9 kN/m and 10.3 kN/m respectively) as well as a Tensar BX-1200 biaxial geogrid (5% strain 10.3 kN/m) were used for reinforcement. All materials were placed at the base/subgrade interface. A 550 kPa pressure was applied at a rate of 0.5 Hz through a stationary steel plate 30 cm in diameter. Loading was commenced until 25 mm of rut depth was obtained.

The control sections deformed 12.5 mm after only 25 cycles which may imply that the control sections were underdesigned. The two geotextiles performed better than the geogrid section (TBR's of 6,7 and 3 respectively). The authors attributed this to mixing of the subgrade/base. The geotextile sections failed (25 mm of rut) after about 1200-1400 cycles which also implies that those sections were underdesigned.

Another field-scale series of reinforced flexible pavements was constructed by Brandon et al. (1995). Nine experimental sections were constructed over a sandy-silt (ML) material with an approximate CBR of 7. The AC thickness was 89 mm and base thicknesses ranged from 100-200 mm. Pressure cells, gypsum blocks (moisture content), and soil strain gages were placed in the base and subgrade layers. AC strain gages were placed in the asphalt layer. Core samples taken from the AC layer of the sections ranged from 78 mm to 99 mm thick. Table 2.2 gives section data for the nine 15 meter long test sections. Three sections had missing thickness data for cut cores (sections 2,6, and 8),

which were geotextile, geogrid, and geotextile reinforced sections respectively. Survey measurement of section 8 indicated a maximum AC thickness of 128 mm.

Table 2.2 Test section data from Brandon et al. (1995).

Section	Geosynthetic	AC thickness (mm) <sup>a</sup>	Base thickness (mm)
1	Unreinforced	77.7	102
2	Geotextile	N/A	102
3	Geogrid	99.0	102
4	Unreinforced	97.8	152
5	Geotextile	90.7	152
6	Geogrid	N/A	152
7	Unreinforced	88.9	203
8	Geotextile	N/A	203
9	Geogrid	85.6	203

<sup>a</sup> Thickness reported from AC cores.

N/A = Not Available

Brandon et al. (1996) presented results from the field-scale experiments. Strain gages were placed on the bottom side of the geotextile and geogrid specimens. Survivability ranged from 6% on the geotextile specimens to 28% for the geogrid foil strain gages over the first eight months. Strain gage results were presented in Bhutta et al. (1998). Strain results were few in number (one geotextile gage and one geogrid gage) and were presented for the perpendicular direction of traffic.

Rut depth versus time measurements were also presented in Bhutta et al. (1998). Results are a bit difficult to interpret for the first year, due to missing data for the first two to three months of operation. By November 1997 (testing commenced August 1994), the control section with 100 mm of base performed very poorly with respect to the corresponding reinforced sections. The textile performed a bit better (by 4 mm) than the

geogrid reinforced section. For the thicker 150 mm base, sections 4-6 and 7-9 were performing about the same.

By November 1997, the geogrid reinforced (section 6) had performed the best, while the geotextile reinforced (section 8) performed a bit worse. Interestingly, one of the control sections (either 4 or 9) performed better than any sections from December 1994 to approximately May 1996, and then began to accelerate rut depth. Measurements for these two control sections are not shown past October 1996. It is also difficult to determine how the variations in AC thickness shown in Table 2.2 affected outcomes of the experimental sections.

Appea et al. (1998) reported results from the experimental program of Brandon et al. (1995) investigating the use of FWD results to predict the separation/contamination function of geotextiles and geogrids. A modulus back calculation program MODULUS was used in conjunction with KENLAYER and ELSYM5 to obtain a transition layer near the subgrade/base interface which was interpreted to be contaminated from cyclic moving wheel loads. The authors stated that geotextiles in the sections provide the separation function while geogrids partially provide that function. Between experimental section 1 (control) and experimental section 3 (geogrid), it appeared that the development of the transition layer (contamination), started lower with the geogrid (0 mm for the geogrid versus 13 mm for the control section), but increased at a faster rate than the control section. This difference occurred up to a period of one year where afterwards the two sections were approximately equal. From this point on, both sections appeared to have

no mixing occurring, which may be due to increasing subgrade strength due to moisture loss or consolidation.

### Conclusions

From the previous experimental studies, the promise of geosynthetics for reinforcement of the base layer remains promising (Moghaddas-Nejad & Small, 1996; Cancelli et al., 1996; Collin et al., 1996; Webster, 1992; Miura, 1990; and Kinney et al., 1998). Other studies (Halliday & Potter, 1984; Barksdale, 1989; and Brandon et al., 1995) have shown mixed results. These mixed results may be based on construction techniques or may be based on material parameters such as subgrade strength. However, the experimental studies have indicated that results are very dependent on the following: layer thickness (particularly the base layer), layer stiffness (particularly the subgrade), geosynthetic type, and geosynthetic placement within the base layer. It also appears from the literature that the mechanisms at work are not well understood because they are not easily quantified. Many efforts (Moghaddas-Nejad & Small, 1996; Cancelli et al., 1996; Collin et al., 1996; Webster, 1992; Kinney et al., 1998; and Brandon et al., 1995), have instrumented the AC surface and the top of the subgrade layers, but with a limited number of instruments that could not describe the stress/strain behavior in light of reinforcement. Instrumenting the geosynthetic with strain gages is another way to more accurately describe the mechanisms involved. In addition, construction quality control must be maintained to high standards for research attempts.

From the previous studies, it appears that geosynthetics are well suited for reinforcement in conditions of soft subgrades ( $\text{CBR} < 8.0$ ), and that both geogrids and geotextiles have merits in certain situations. Stiffer materials appear to function better (higher lateral restraint), but the benefits may be offset by the additional costs of stronger materials. Reinforcement also appears to function best when placed at the subgrade/base interface or in the bottom half of the base. It remains to be seen if placement within the base is feasible for construction with thin bases. Additionally, the reinforcement potential is maximized with thin (100-150 mm) to medium thin base courses (300-375 mm).

The research at Montana State University will try to address some of the main variables discussed previously, with an attempt to accurately describe, in a mechanistic way, the behavior of reinforced sections with both geogrids and geotextiles. The research will also attempt to describe reinforcement benefits in a strong subgrade material ( $\text{CBR} = 15-20$ ). Chapter 3 presents the experimental apparatus and techniques used in constructing the test sections.

## CHAPTER THREE

### EXPERIMENTAL METHODS

#### Introduction

This chapter provides information on the procedures used in constructing, instrumenting, and testing the experimental pavement sections. A total of 21 sections were completed to provide a large database of information that could be used to describe the reinforcement effects of incorporating a geosynthetic into the base course layer of a flexible pavement system. Nine sections were constructed using a silty-sand subgrade and twelve sections were constructed using a clay subgrade. One of the twelve clay sections was termed a "preliminary" section, which contained limited instrumentation designed to provide information on instrument response. Terminology used for naming sections in this report is as follows: 1) Silty-Sand Subgrade tests are termed "SSS", 2) Clay Subgrade tests are termed "CS", and 3) The Preliminary Clay Subgrade test was termed "PCS". Test sections are then numbered in the order performed.

Test section variables studied and implemented into the experimental program consisted of subgrade type, geosynthetic type, location within the base course, and base course layer thickness. Construction of the 21 test sections included in this report began in December, 1996 and terminated in November, 1998.

## Laboratory Test Facility

### **Test Box and Loading Apparatus**

A test box was constructed having inside dimensions of 2 meters in width and length and 1.5 meters in height. Walls consisted of 150 mm thick reinforced concrete. The bottom was left open to allow for any drainage that may occur from the subgrade. The front wall is removable in order to facilitate removal for excavation of the test sections. The front wall is attached by large 25 mm diameter bolt and nut assemblies. The box was constructed with reinforced concrete in order to minimize lateral movement when the dynamic 40 kN load was applied to the pavement surface. Figures 3.1 and 3.2 show an isometric view and front view schematics of the test box and loading apparatus.

I-beams were set into the concrete and served as a base for the loading frame. The I-beams also allowed the load-frame to be moved such that the load could be applied at various locations across the pavement surface. The usefulness of a movable load is discussed later. The loading apparatus consists of two I-beams set perpendicular to the I-beams set into the concrete walls of the box.

The load actuator is placed between the two I-beams. The loading assembly consists of an air-operated actuator with a 305 mm bore connected to a 50 mm diameter steel rod. This steel rod is approximately 300 mm long and is rounded at its bottom end. The rounded portion of the loading rod fits into a cup welded on the load plate. This "ball and joint" connection provides some flexibility of rotation between the load plate and the loading rod.



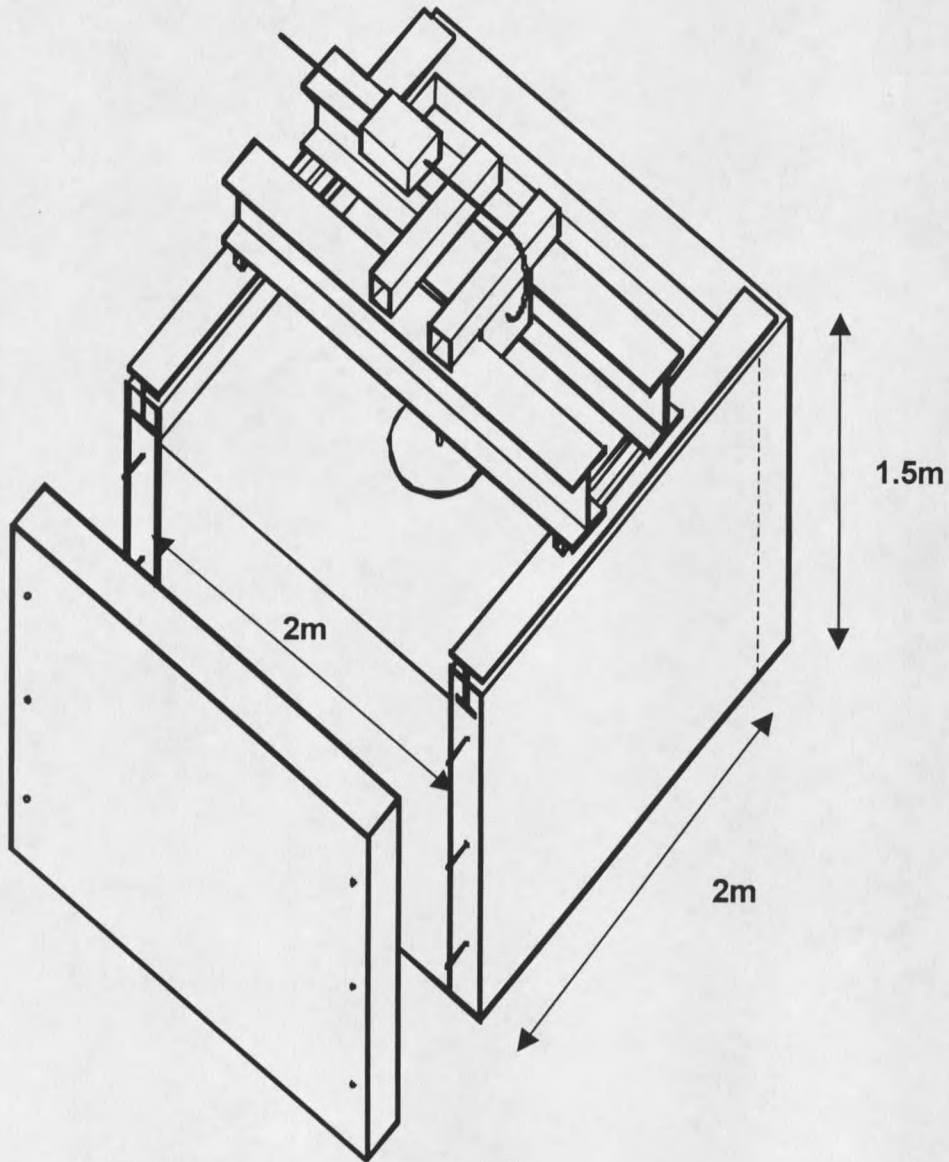


Figure 3.1. Isometric view of the test box and loading apparatus.

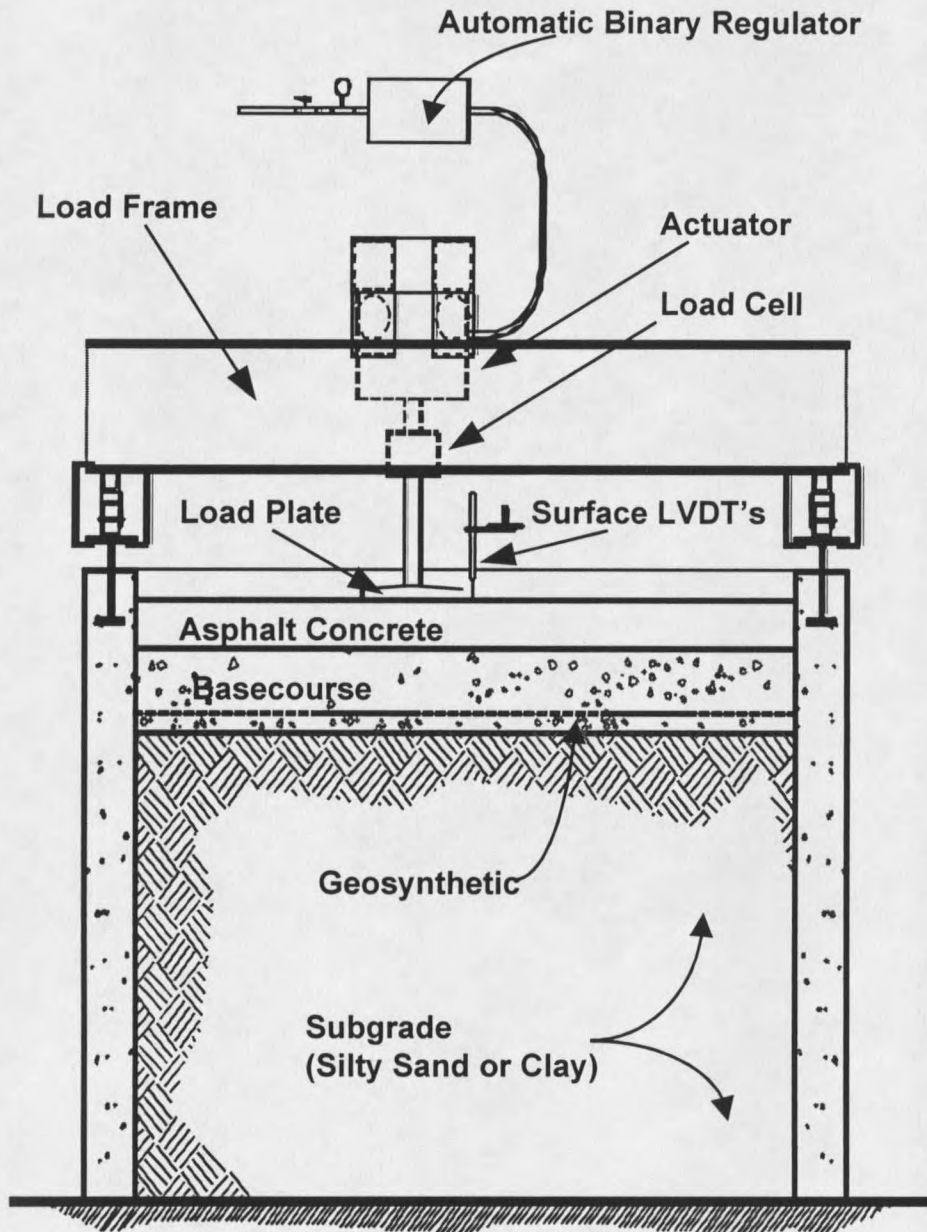


Figure 3.2. Schematic of apparatus components and pavement layers. Note: Load not shown in center of box to illustrate movement capabilities.

A circular, 305 mm diameter load plate with a thickness of 25 mm was machined out of steel. A 4 mm thick, waffled butyl-rubber pad was placed beneath the load plate in order to provide a uniform pressure and avoid stress concentrations along the plate's perimeter. Figures 3.3 and 3.4 show pictures of the test box and the load plate resting on the pavement surface.

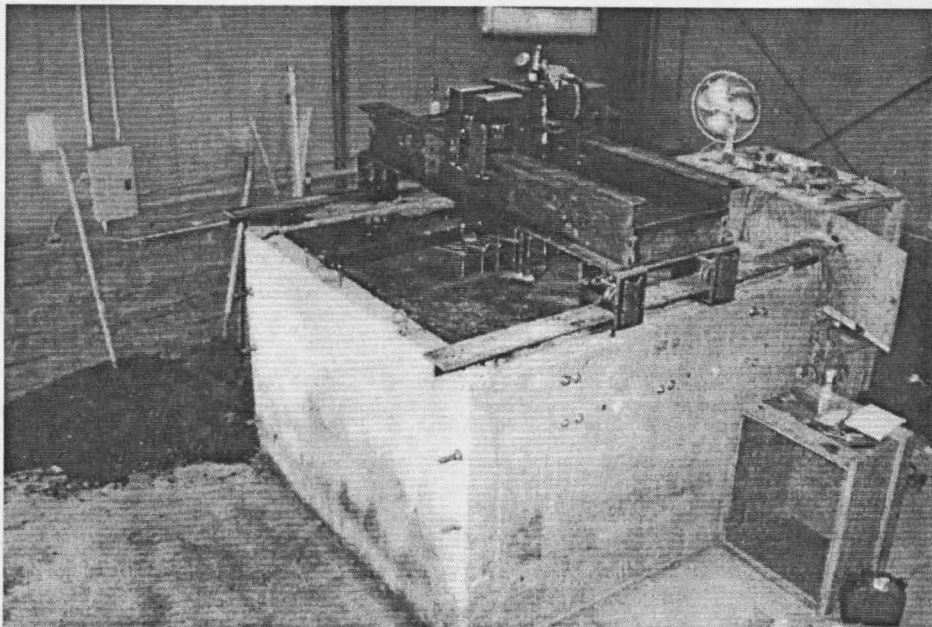


Figure 3.3. Overall picture of the pavement test facility.

### **Instrumentation**

Instrumentation used in the test sections allows for examination of reinforcement mechanisms occurring during dynamic loading and a mechanistic interpretation of pavement response. Results solely based on asphalt concrete surface deformation (rut) are not sufficient and are more valuable when combined with experimental results that describe individual material layer behavior inside the test section.

The test sections contained as many as 100 instruments measuring stress, strain, temperature, and moisture content. Instrumentation has been categorized into instruments measuring asphalt surface deflection, tensile strain in the asphalt concrete, stress and strain in the base course and subgrade, strain on the geosynthetic, and general instrumentation measuring water content and temperature of the pavement system. The next five sections will describe the different categories of instrumentation used in the test sections.

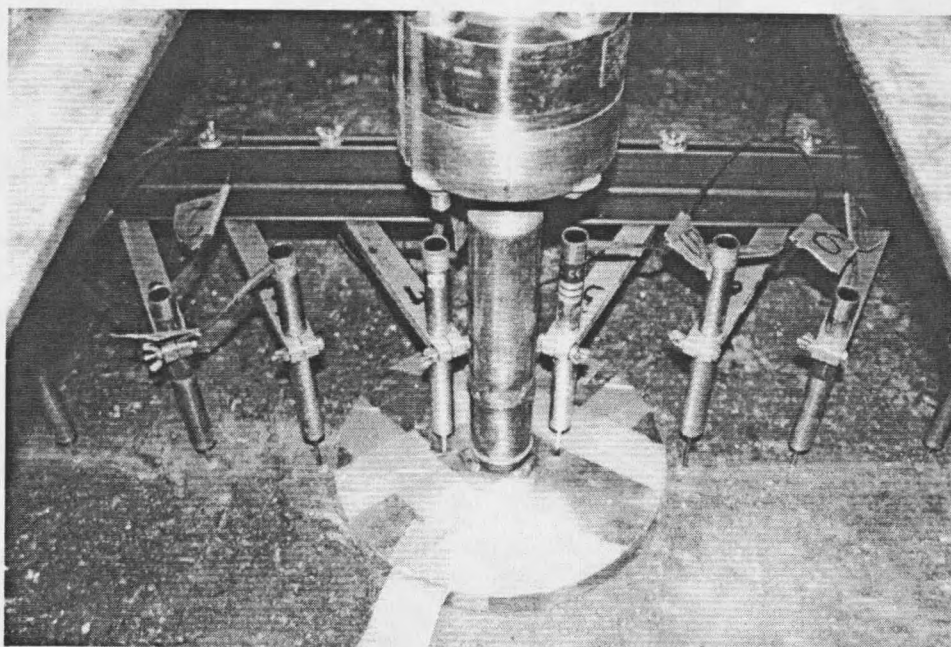


Figure 3.4. Closeup of the 305 mm diameter load plate, load cell (top), and surface LVDT's resting on the pavement surface.

Asphalt Concrete Instrumentation. Linear variable differential transducers (LVDT's) were placed vertically on the asphalt concrete surface to measure surface deflection during loading. These gages are manufactured by RDP Electronics (Pottstown, PA). Two different gages were used with ranges of 25 mm and 50 mm. The

LVDT's with the greatest range were placed closest to the center of the load plate where the largest surface deformations occurred. The other gages were placed at increasing radial distances (100 mm spacings) from the load centerline. These instruments are shown in their respective orientation on the asphalt surface in Figure 3.4. The surface LVDT's provide a smooth asphalt surface deflection bowl (asphalt deflection across the pavement surface) for a given load pulse and an accumulation of permanent deformation with load cycle number. A typical deflection bowl is presented in Figure 3.5.

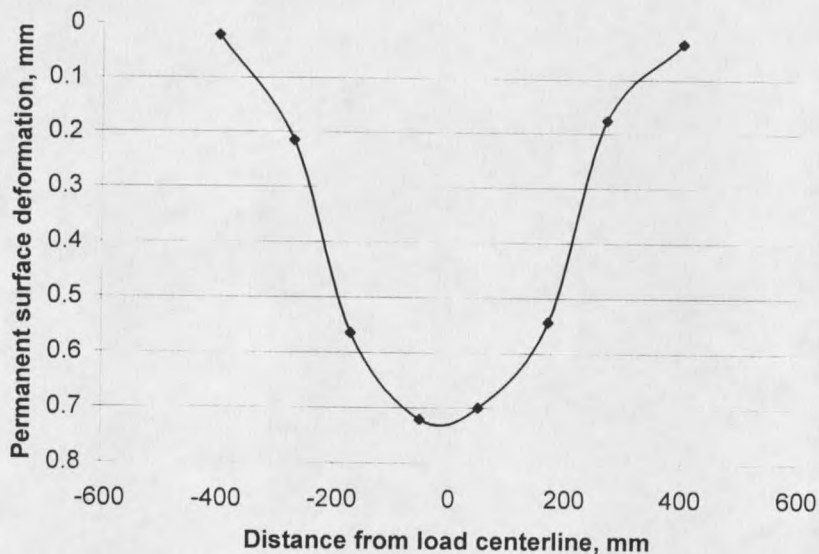


Figure 3.5. Typical plot of permanent surface deformation after 5 load cycles for test section CS1.

H-type, PAST (PAVement Strain Transducer) asphalt strain gages manufactured by Dynatest, Inc. (Ojai, CA), were used to measure tensile strain in the bottom of the asphalt concrete. The gages measure 135 mm in length and 70 mm in width and are shown in Figure 3.6. These gages have a range of approximately 1500 microstrain

(0.15%). The inside of the gage consists of a strain gage embedded in a strip of glass-fiber reinforced epoxy that has a high flexibility and relatively low strength. A multi-layer coating protects the gage from chemical effects. The average elastic modulus of the cell body is 2.2 MPa, resulting in a low “strain force” of 0.11 N/microstrain. Hence, material surrounding the gage is not highly influenced by installation of the strain gage. Fatigue life of the gage is theoretically estimated at  $1 \times 10^6$  cycles. Figure 3.7 illustrates the various coatings and components of the AC strain gage.

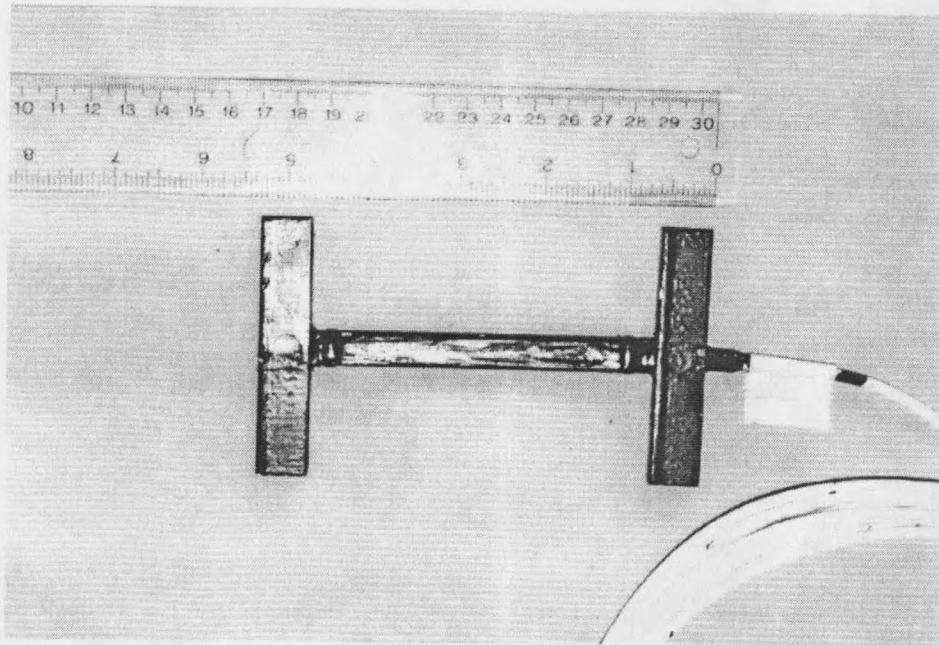


Figure 3.6. Asphalt concrete strain gage.

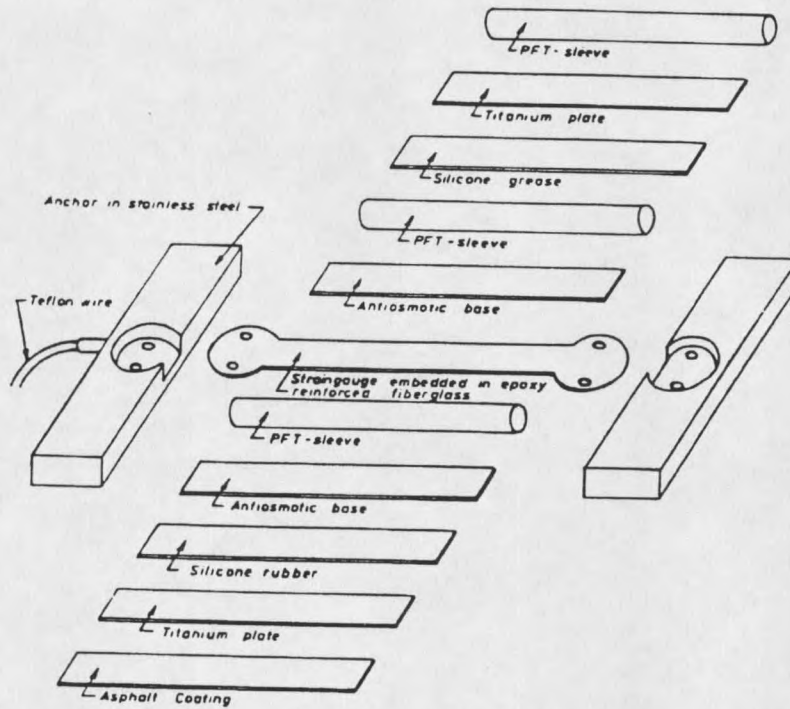


Figure 3.7. Different components of the Dynatest H-type PAST (Dynatest, 1991).

Geosynthetic Instrumentation. Foil strain gages were mounted to geogrid and geotextile samples in order to quantify in-situ strain behavior during pavement loading. Measuring strain on the geosynthetic provides another means of quantifying mechanisms associated with geosynthetic reinforcement. Small, 18 mm long strain gages (Micromeritics Group, Inc., model EP-080500GB-120) were used for the geogrid specimens. These gages have a range of approximately 20% strain, and a fatigue life of approximately 10,000 cycles under 0.1% dynamic strain. 110 mm long foil strain gages (Micromeritics Group, Inc., model EP-08-40CBY-120) were attached to geotextile specimens. These gages also have a range of approximately 20% strain, but only 10% of the range was utilized for greater sensitivity. Figure 3.8 shows the two foil strain gages

used in this study. Attachment of the foil strain gages to geosynthetic samples is discussed later in this chapter under the section "Test Section Construction".

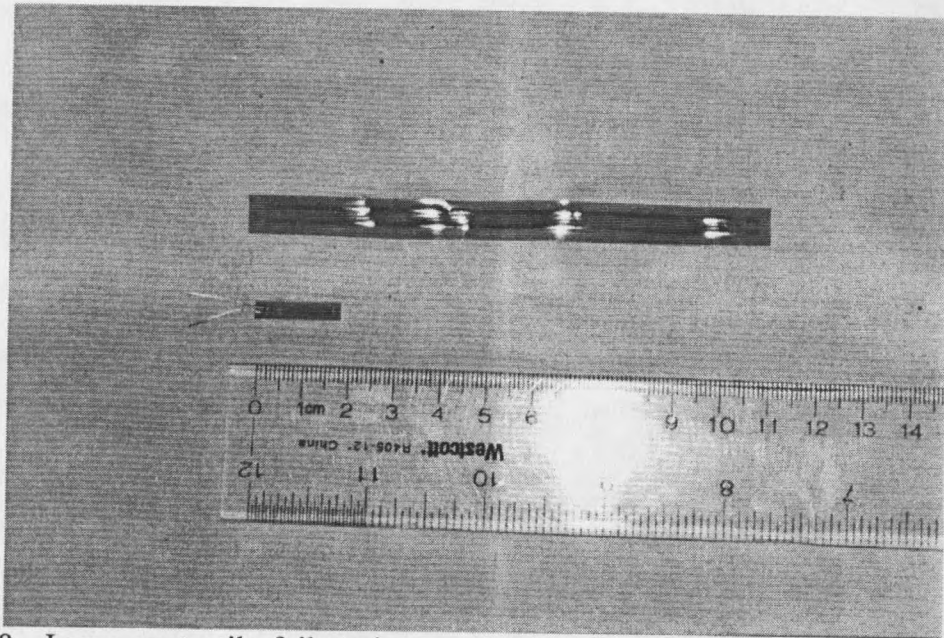


Figure 3.8. Large geotextile foil strain gage (top) and smaller geogrid foil strain gage (bottom).

Base Course and Subgrade Instrumentation. Stress cells were placed in both the base course and the subgrade in order to quantify the dynamic stress behavior of the system. The stress cells were obtained from Dynatest, Inc., (Ojai, CA). The cell utilizes a thin membrane (0.5 mm thick) that covers a layer of fluid. Fluid pressure is measured by a pressure transducer (fully-bridged strain gage) inside the cell. The cells are coated with epoxy and sand to insure proper bonding to soil materials. Fatigue life is listed at  $3 \times 10^6$  cycles. Two types of stress cells were utilized in the test sections having different operating ranges. Type A stress cells were placed in both the base course and subgrade having a range of 10-200 kPa. Type B stress cells having a maximum range of 800 kPa,



were placed in a horizontal orientation (measuring vertical stress) in the base course directly beneath the load plate. The type B cells were placed directly beneath the load because of higher pressures expected. A typical stress cell is pictured in Figures 3.9 and 3.10.

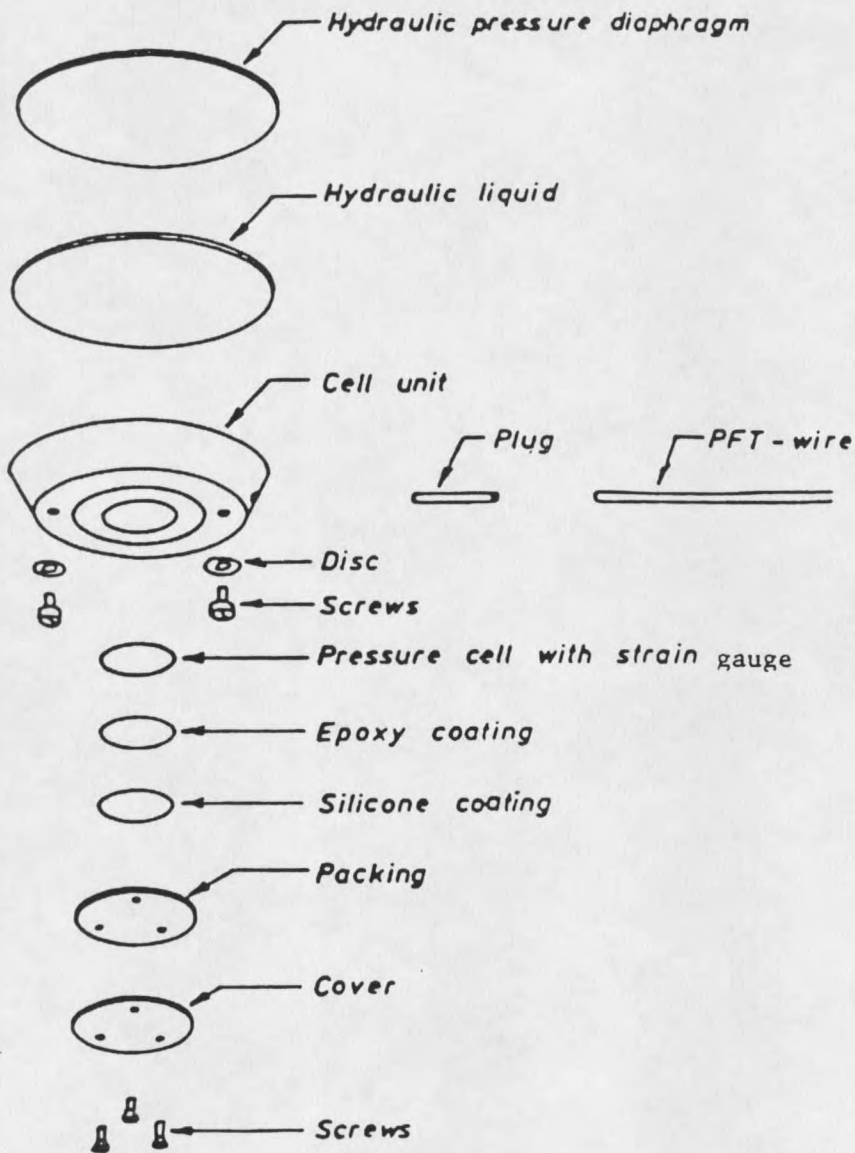


Figure 3.9. Dynatest SOil Pressure Transducer (SOPT) (Dynatest, 1991).

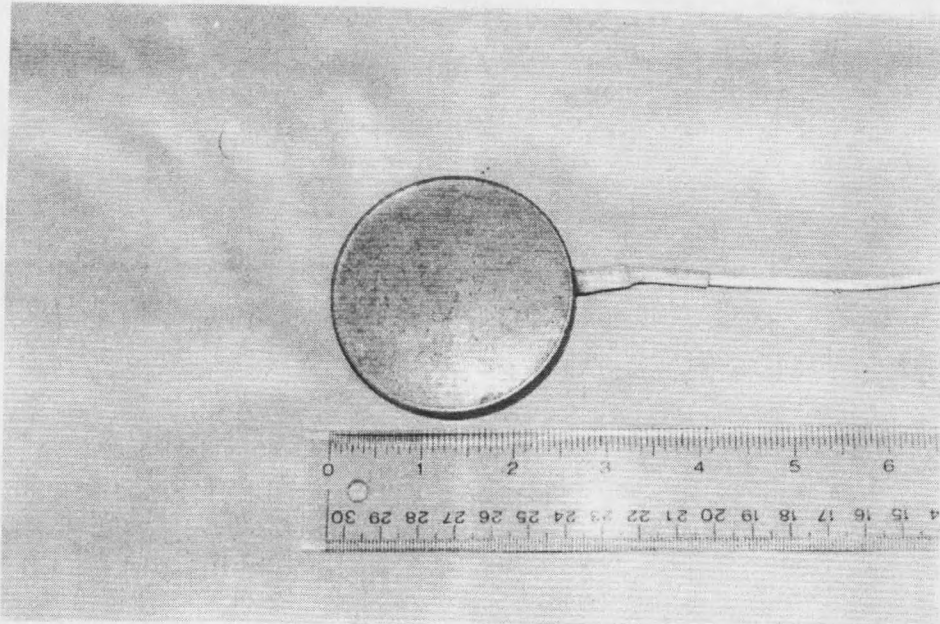


Figure 3.10. Typical stress cell.

Strain in both the base and subgrade was measured by alternating current (AC) LVDT's fitted with steel end plates measuring 50 mm x 15 mm x 5 mm in thickness. The LVDT's (model D5/400W) were obtained from RDP Electronics (Pottstown, PA). The gages have a nominal gage length of 70-80 mm, which corresponds to a 0.2-10% strain range depending on the electronic amplification used for the sensor. A typical LVDT used in test sections is shown in Figure 3.11.

General Instrumentation. Temperature probes from RDP Electronics (Pottstown, PA), were used in certain tests to correct stress cell readings for temperature variations. It was noticed that some stress cells drifted by as much as 2-5 kPa when a temperature variation of 8.3 degrees Celsius occurred. The temperature probes allowed the stress variations due to temperature to be corrected, especially in the summer test sections



















































































































































































































































































































































































































































